Bioactive Materials 7 (2022) 39–46

Contents lists available at ScienceDirect

Bioactive Materials

journal homepage: www.sciencedirect.com/journal/bioactive-materials

Antiviral adsorption activity of porous silicon nanoparticles against different pathogenic human viruses

Liubov A. Osminkina [a,b,*], Svetlana N. Agafilushkina [a], Ekaterina A. Kropotkina [c], Nikolay Yu Saushkin [a,d], Ivan V. Bozhev [a,e], Sergei S. Abramchuk [a,f], Jeanne V. Samsonova [a,d], Alexandra S. Gambaryan [b]

[a] Lomonosov Moscow State University, Physics Department, Leninskie Gory 1, 119991, Moscow, Russian Federation
[b] Institute for Biological Instrumentation of Russian Academy of Sciences, 142290, Pushchino, Moscow Region, Russian Federation
[c] Chumakov Federal Scientific Center for Research and Development of Immune-and-Biological Products, Russian Academy of Sciences, 108819, Moscow, Russian Federation
[d] Lomonosov Moscow State University, Faculty of Chemistry, Leninskie Gory 1, 119991, Moscow, Russian Federation
[e] Quantum Technology Center, Lomonosov Moscow State University, Physics Department, Leninskie Gory 1, 119991, Moscow, Russian Federation
[f] A.N. Nesmeyanov Institute of Organoelement Compounds of Russian Academy of Sciences, Vavilova 28, 119991, Moscow, Russian Federation

ARTICLE INFO

Keywords:
Pathogenic human viruses
Porous silicon nanoparticles
Virus
Antiviral activity
Virucide

ABSTRACT

New viral infections, due to their rapid spread, lack of effective antiviral drugs and vaccines, kill millions of people every year. The global pandemic SARS-CoV-2 in 2019–2021 has shown that new strains of viruses can widespread very quickly, causing disease and death, with significant socio-economic consequences. Therefore, the search for new methods of combating different pathogenic viruses is an urgent task, and strategies based on nanoparticles are of significant interest. This work demonstrates the antiviral adsorption (virucidal) efficacy of nanoparticles of porous silicon (PSi NPs) against various enveloped and non-enveloped pathogenic human viruses, such as Influenza A virus, Poliovirus, Human immunodeficiency virus, West Nile virus, and Hepatitis virus. PSi NPs sized 60 nm with the average pore diameter of 2 nm and specific surface area of 200 m^2/g were obtained by ball-milling of electrochemically-etched microporous silicon films. After interaction with PSi NPs, a strong suppression of the infectious activity of the virus-contaminated fluid was observed, which was manifested in a decrease in the infectious titer of all studied types of viruses by approximately 10^4 times, and corresponded to an inactivation of 99.99% viruses *in vitro*. This sorption capacity of PSi NPs is possible due to their microporous structure and huge specific surface area, which ensures efficient capture of virions, as confirmed by *ELISA* analysis, dynamic light scattering measurements and transmission electron microscopy images. The results obtained indicate the great potential of using PSi NPs as universal viral sorbents and disinfectants for the detection and treatment of viral diseases.

1. Introduction

New pathogenic viruses can arise in humans from existing human viruses or from animal viruses. The current global pandemic SARS-CoV-2 has shown that new strains of pathogenic viruses can spread very quickly and, due to the lack of effective antiviral drugs and rapid vaccine development methods, cause illness and death of millions of people, which in turn leads to significant negative socio-economic consequences. Therefore, the search for new methods of combating various pathogenic viruses is an urgent task, and strategies based on nanoparticles are of significant interest.

The unique physicochemical and structural properties of nanoparticles (NPs) make them very attractive for various biomedical applications [1–4]. NP-based antiviral therapeutics can inhibit cell-virion interaction, the replication of genetic material, or the release of newly formed virions. Another strategy for stopping viral infection is the virucidal action of NPs to inactivate or destroy the virus itself, and various NPs have been proposed [1]. NPs of different materials, and

Peer review under responsibility of KeAi Communications Co., Ltd.
* Corresponding author. Lomonosov Moscow State University, Physics Department, Leninskie Gory 1, 119991, Moscow, Russian Federation.
E-mail address: osminkina@physics.msu.ru (L.A. Osminkina).

https://doi.org/10.1016/j.bioactmat.2021.06.001
Received 7 August 2019; Received in revised form 15 May 2021; Accepted 2 June 2021
Available online 16 June 2021

especially metal nanoparticles, are well-known for their activities against a diversity of viruses [5,6]. Thus, NPs obtained from silver (Ag NPs), have received tremendous attention for inhibiting various types of viruses [7–11]. Gold nanoparticles (Au NPs) have been proposed as anti-viral systems taking advantage of the core material and/or the ligands shell [6]. However, most research attempts to destroy the virus using NPs, but the challenge is to selectively damage the virus without affecting its host. Moreover, according to various reports, metal NPs could be the carriers of numerous biological risks. It was observed that metal and metal oxide nanoparticles implanted into mammalian cells caused alteration of the normal function of mitochondria, the increase of membrane permeability and the generation of reactive oxygen species which resulted in oxidative stress and cellular damage [12–15]. Also, because of the non-biodegradability of such metal nanoparticles, it is difficult to envision where these nanoparticles would find a niche for actual therapy [16].

Porous silicon nanoparticles (PSi NPs) have now demonstrated great potential for their use in biomedicine, especially as effective drug delivery systems [17–19]. The advantages of using PSi NPs as antiviral agents are primarily associated with their low cytotoxicity [20], when even bare PSi NPs do not show cytotoxicity *in vitro* up to concentrations of 0.7 mg/ml during 2 weeks of incubation with various cells [17], and biodegradability because of gradual dissolution in biological liquids accompanied by formation of non-toxic silicic acid [17–21]. There are several methods for preparing PSi NPs. Among them, the most widely used is the mechanical milling or ultrasound fragmentation of PSi films [22]. Usually, PSi films are produced by top-down method of electrochemical etching of a crystalline p-type silicon wafer in hydrofluoric acid (HF) and ethanol solutions [23]. At the same time, by tailoring the etching current density, crystalline silicon substrate doping level and the concentration of the etching solutions used, one can tunable both the pore sizes and the sizes of silicon walls of the resulting porous film [24–26]. PSi films as well as PSi NPs are generally classified according to the IUPAC (International Union of Pure and Applied Chemistry) principle, which defines the type of porous material depending on the pore size. Thus, PSi films and NPs with a pore size $\leq$2 nm are considered microporous, from 3 to 50 nm are mesoporous, and more than 50 nm are macroporous [27]. Previously we report that PSi NPs can act as efficient scavengers of human immunodeficiency virus (HIV) and respiratory syncytial virus (RSV): a strong suppression of the viral activity in the presence of PSi NPs have been revealed *in vitro* [28]. Also, the possibility of creating electrical and optical sensors based on PSi films for virus detection was shown earlier in works [29,30]. Thus, based on the unique structural and bio-properties of silicon nanoparticles, the study of their virucidal activity against pathogenic human viruses is of both scientific and applied interest.

Influenza virus (Flu, *Orthomyxoviridae* family) mostly spherical particles with 80–120 nm in diameter. Membrane glycoproteins, hemagglutinin and neuraminidase are the two most abundant proteins on the surface of influenza A virus particles [31]. Influenza viruses infect many vertebrates, while influenza A, B and C viruses (IAV, IBV and ICV) infect humans. The high mutation rate avoids immunity. IAV from different host species can 'reassort' their segmented genomes, producing pandemic strains that are antigenically novel but otherwise well adapted to humans [32]. Among the various causative agents of acute respiratory viral infections, the influenza virus occupies a special place. In addition to the usual seasonal epidemics, pandemics of a completely new influenza virus occur periodically, the level of pathogenicity of which cannot be predicted. The 1918 influenza virus pandemic claimed the lives of about 50 million people worldwide [33].

Poliomyelitis virus, poliovirus (*Picornaviridae* family), is a spherical, non-enveloped virus, with a diameter of approximately 30 nm [34]. The poliomyelitis virus is transmitted from person to person by the fecal-oral route, and mainly affects children under the age of five. The virus multiplies in the intestines, from where it can enter the nervous system through the bloodstream, potentially causing paralysis [35]. Polioviruses are the causative agents of widespread poliomyelitis epidemics in the twentieth century. The Global Polio Eradication Initiative (GPEI) has achieved now >99% reduction in the global annual incidence of poliomyelitis since the program began in 1988, but polio cases are still being detected in some countries due to lack of vaccines or vaccine refusal [36].

The average particle size of the human immunodeficiency virus (HIV, *Retroviridae* family) is 145 nm, they are generally spherical and contain a characteristic cone-shaped core that encases the viral RNA and replication proteins [37]. HIV is a virus that attacks the body's immune system. To infect cells, the HIV protein envelope (Env) binds to the primary cellular receptor CD4 and then to a cellular coreceptor [38]. If HIV is not treated, it can lead to AIDS (acquired immunodeficiency syndrome). With 1.7 million people becoming newly infected with HIV in 2019, there is still an urgent need to develop new ways of preventing HIV and make them available so that people can protect themselves from the virus [39].

West Nile virus (WNV) has icosahedral symmetry and is about 50 nm in diameter with no surface projections or spikes, which are prominent on other envelope-containing viruses such as influenza and HIV [40]. The protein shell of the virus corresponds to the glycoprotein E and a small membrane protein M [41]. WNV, a member of the *Flavivirus* genus, transmitted primarily by *Culex* mosquitoes to vertebrate hosts. Flaviviruses include members such as dengue virus, yellow fever virus, and tick-borne encephalitis virus, causes fever that can progress to life-threatening encephalitis [40,41]. There is currently no vaccine available for humans and the virus continues to spread [42].

Hepatitis A virus (HAV), is a non-enveloped spherical virus, viral family *Picornaviridae*, about 30 nm in size, with cubic symmetry (panel) [43,44]. Hepatitis A virus (HAV) is a pathogenic, hepatotropic picornavirus transmitted by the fecal-oral route or consumption of contaminated food or water. HAV is unique among picornaviruses in targeting the liver and continues to be a source of mortality despite a successful vaccine [45,46]. Since 2016, the United States has experienced person-to-person HAV, unprecedented in the vaccine era. The proportion of cases hospitalized in these outbreaks exceeds historical national surveillance data [47].

Viral contamination is a major problem in the production of biopharmaceuticals [48]. Water pollution by viral pathogens contributes to the rapid spread of infections in animals and humans [49]. Virus clearance is a laborious process that is usually achieved by removal and/or decontamination, and different viruses have different susceptibility to the methods used [48]. Silicon is the second most abundant element in the Earth's crust after oxygen, and its nanoforms also do not have a toxic effect on people and nature. Thus, the use of silicon nanoparticles for inactivation of viruses is an attractive idea.

In this work, the universal antiviral adsorption properties of PSi NPs against pathogenic human viruses were studied using the example of viruses of various sizes, shapes, with and without an envelope: H1N1 influenza A, Poliovirus, Human immunodeficiency virus, West Nile virus and Hepatitis A virus. A strong decrease in viral activity after interaction with nanoparticles has been demonstrated for all types of viruses used.

2. Materials and methods

2.1. Synthesis of porous silicon flakes and nanoparticles

Aqueous suspensions of porous PSi NPs were fabricated by mechanical grinding of porous silicon (PSi) films formed by the electrochemical etching of boron-doped (specific resistivity of 10 Ω cm) (100)-oriented crystalline silicon (c-Si) wafers in a solution of HF (50%): C_2H_5OH = 1:1 at current density of 50 mA/cm^2 and etching time of 60 min. To provide electrical contact, a thin layer of aluminum was deposited on the back side of the c-Si wafers. Prior to grinding, the porous films were detached from c-Si substrates by applying a short pulse of the etching current with density of 500 mA/cm^2. This caused

the PSi film to lift off with the formation of flakes. The grinding was done by milling the flakes in deionized water for 20 min (15 min with 3 mm ZrO_2 balls, 5 min with 100 μm ZrO_2 balls) under rotation speed of 1000 rpm by using a FRITSCH « Pulverisette 7 premium line » ball mill machine. Schematic representation of PSi NPs preparation is shown in Fig. 1. Then freshly prepared suspensions were centrifuged at 2000 rpm for 2 min at room temperature. The resulting supernatant was used to study the structural properties of nanoparticles and their interaction with various viruses.

2.2. Sample's characterization

Structural analysis of the samples was carried out by field emission scanning electron microscopy (SEM, Carl Zeiss ULTRA 55 FESEM), as well as transmission electron microscopy (TEM, LEO912 AB OMEGA). The samples of PSi NPs for TEM studies were prepared by deposition of a drop of the aqueous suspension of nanoparticles on the standard carbon-coated gold TEM-grids followed by their drying in air for 10 min. TEM images were processed with ImageJ Software to obtain the particle size distribution. The dynamic light scattering (DLS) measurements were performed with a Malvern Zetasizer Nano ZS instrument to determine the size distribution and zeta potential (ZP) of nanoparticles in aqueous suspensions. The DLS measurements were implemented for the nanoparticles' diluted to a concentration of 0.01 mg/ml.

Specific surface area and pore size distribution of nanoparticles were measured by means of nitrogen adsorption/desorption using a Quantachrome NOVA 4200e apparatus. Before the adsorption/desorption measurements, the aqueous suspensions of PSi NPs were freeze-dried by lyophilization process for several hours. The surface area was evaluated by the Brunauer–Emmett–Teller (BET) method, and the pore size distribution was calculated by using the Barret–Joyner–Halenda (BJH) method.

The surface composition of nanoparticles was studied by using a Fourier-transform infrared (FTIR) spectrometer (Bruker IFS 66v/S) with a germanium prism of the attenuated total reflection unit. Before recording FTIR spectra, the suspensions were air-dried on the prism surface. The FTIR measurements were done at room temperature in air.

2.3. Assessment of PSi flakes and PSi NPs antiviral adsorption activity by ELISA

A suspension of PSi flakes or PSi NPs in 0.01 M K-phosphate buffer supplied with 0.15 M NaCl, pH = 7.4 (concentration 0.1–5 mg/ml) was mixed with a solution of Influenza A/New Caledonia/20/99 (H1N1) virus (0.5, 1, 2.5 and 5 μg/ml) in the ratio of 100 μl:100 μl and incubated on a shaker (IKA® VXR basic Vibrax® orbital shaker) for 5–60 min. The virus purification process for *ELISA* experiments is described in the Supplementary data file (SD). Then the obtained suspension was centrifuged for 2 min at 2000 rpm (Microspin-12 Biosan) and 100 μl of the supernatant was transferred into the wells of a polystyrene plate with preabsorbed specific monoclonal antibodies against the used stain of H1N1 influenza virus. The plate was incubated for 1 h at 37 °C. Then the plate was washed with 3 × 200 μl of wash buffer (PBS with 0.05% Tween-20), 100 μl of fetuin-horse radish peroxidase conjugate solution was added and then incubated for 1 h at 4 °C. After washing, 100 μl of a substrate solution containing 3,3′,5,5′-tetramethylbenzidine was added, after 10–15 min, 100 μl of stop solution (0.1 M sulfuric acid) was added and the optical density was recorded at 450–620 nm. Free virus concentration in supernatant was calculated against the calibration curve obtained for standard solutions of the same H1N1 virus strain (0.05, 0.25, 0.5, 1, 2.5, 5 μg/ml) (SD Fig. S1).

2.4. Characterization of viruses and cell lines used in vitro experiments

Influenza A virus. Strain A/PR/8/1934H1N1. The family Orthomyxoviridae. BHK-21 cell culture (Hamster Kidney).

Poliovirus. Type 1, vaccine strain P1/Sabin. The family Picornaviridae. Vero cell culture (African Green Monkey Kidney).

Hepatitis A virus. Strain IVA. The family Picornaviridae. BHK-21 cell culture (Hamster Kidney).

Human immunodeficiency virus. Type 1 (Strain UGANDAN/ISOLATE U455). The family Retroviridae. MT-2 cell culture (Human T Lymphocyte).

West Nile virus. Strain Ast 986. The family Flaviviridae. BHK-21 cell culture (Hamster Kidney).

Monolayer cultures of BHK-21 and Vero were in DMEM with 10% fetal bovine serum (FBS). Cell culture MT2 was in culture medium RPMI1640 with 10% of FBS. Cells were passaged twice a week. The cells were sown in 24-well plates the day before infection, then washed twice with culture medium, and incubated for 4 h at 37 °C in a 5% CO_2 atmosphere before treatment.

The values of the virus titer are listed in TCID50/ml, that describes the dose required to trigger infection in 50% of cell cultures. Concentrations of viruses in 1 ml of each original virus suspension were about $7{,}5*10^5$ $TCID_{50}$ for Influenza A virus, $5{,}0*10^8$ $TCID_{50}$ for Poliovirus, $5{,}0*10^7$ $TCID_{50}$ Hepatitis A virus, $2{,}5*10^3$ $TCID_{50}$ for Human immunodeficiency virus and 5,0*108 TCID50 for West Nile virus.

The virus purification process is described in the SD.

2.5. The study of the interaction of viruses and nanoparticles using dynamic light scattering

To measure the sizes of the virions, the viral suspension was centrifuged at 15,000 rpm for 30 min, and the supernatant was picked and poured into the DLS cuvette. The described procedure was necessary to get rid of the cell culture components, which do not let observe the existence of virions in the solution.

To demonstrate the interaction of viruses and PSi NPs the 10 times diluted by PBS suspension of Influenza A virus was used. Firstly, the viral suspension was prepared by the method described above. Following this, PBS diluted up to 0.01 mg/ml suspension of PSi NPs was added to the cuvette with virus in ratio 1:1. Finally, the solutions of Influenza A, PSi NPs and their mixture (after 20 min at IKA® VXR basic Vibrax® orbital shaker) were examined via DLS.

2.6. In vitro study of the virucidal properties of PSi NPs

Aqueous suspension of PSi NPs was diluted with culture medium to a concentration of 1 mg/ml with a pH of 7.2 and then 800 μl were mixed with 100 μl of virus suspension (Influenza A virus, Poliovirus, Hepatitis A virus, Human immunodeficiency virus and West Nile virus) and 100 μl of bidistilled water (taken as an interfering substance). The obtained mixtures of PSi NPs and virions were stirred for 20 min at room temperature at IKA® VXR basic Vibrax® orbital shaker. Then, the mixtures

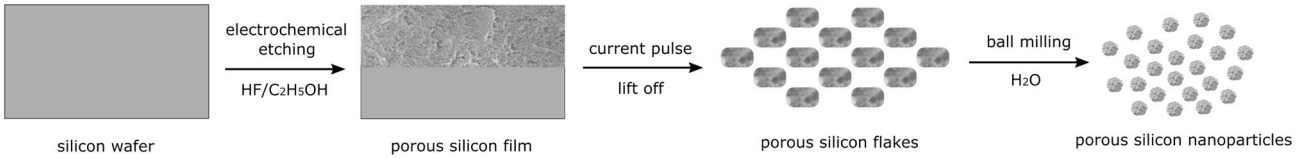

Fig. 1. Schematic representation of PSi NPs preparation by mechanical milling of electrochemically-etched microporous PSi films.

were centrifuged at 2000 rpm for 15 min at room temperature, and the resulting supernatant was used to infect the cells. The control samples were subjected to the same procedures, but instead of a suspension of PSi NPs, the culture medium was added.

Serial 10-fold dilutions of the virus supernatant or PSiNPs&virus supernatant were made and 100 μl of each dilution were inoculated to the wells of the 24-well microtitration plate with an appropriate cell culture. Then the plates were incubated for 4 h at 37C in 5% CO2, washed twice with culture medium and a maintenance medium was added (with 1.2% of FBS). Further incubation of the infected cells at 37 °C was limited by the cytopathic effect of viruses: 5 days for Poliovirus and West Nile virus, 7 days for Influenza A virus, 14 days for Hepatitis A virus and Human immunodeficiency virus. The virus titers were determined using the standard methods [28] and expressed as TCID50/ml.

2.7. Statistics and data analysis

Statistical data were collected and presented as mean ± standard deviation (SD).

2.8. The study of the interaction of viruses and nanoparticles by transmission electron microscopy

PSi NP suspension with concentration of 0.05 mg/ml was mixed 1:1 with Influenza A viral solution (0.1 μg/ml) and stirred for 20 min at IKA® VXR basic Vibrax® orbital shaker. Finally, the suspension was diluted and examined using TEM (LEO912 AB OMEGA), where 2% phosphoric tungstic acid was used for negative staining.

3. Results and discussion

3.1. Structural properties of nanoparticles

Microporous silicon (PSi) films were prepared by the electrochemical etching of boron low-doped crystalline silicon substrates (c-Si). Thickness of the film was in about 7 μm, as revealed by cross-section scanning electron microscope (SEM) image (Fig. 2a). Due to the highly microporous structure of the obtained PSi films (SD Figs. S2a and b), during the procedure of detachment them from the c-Si surface when a short-term high-intensity current pulse was applied, they self-destroyed into flakes. A plan-view SEM image of the obtained PSi flakes presented in Fig. 2b. The mean size of the PSi flakes, obtained by the analysis of the

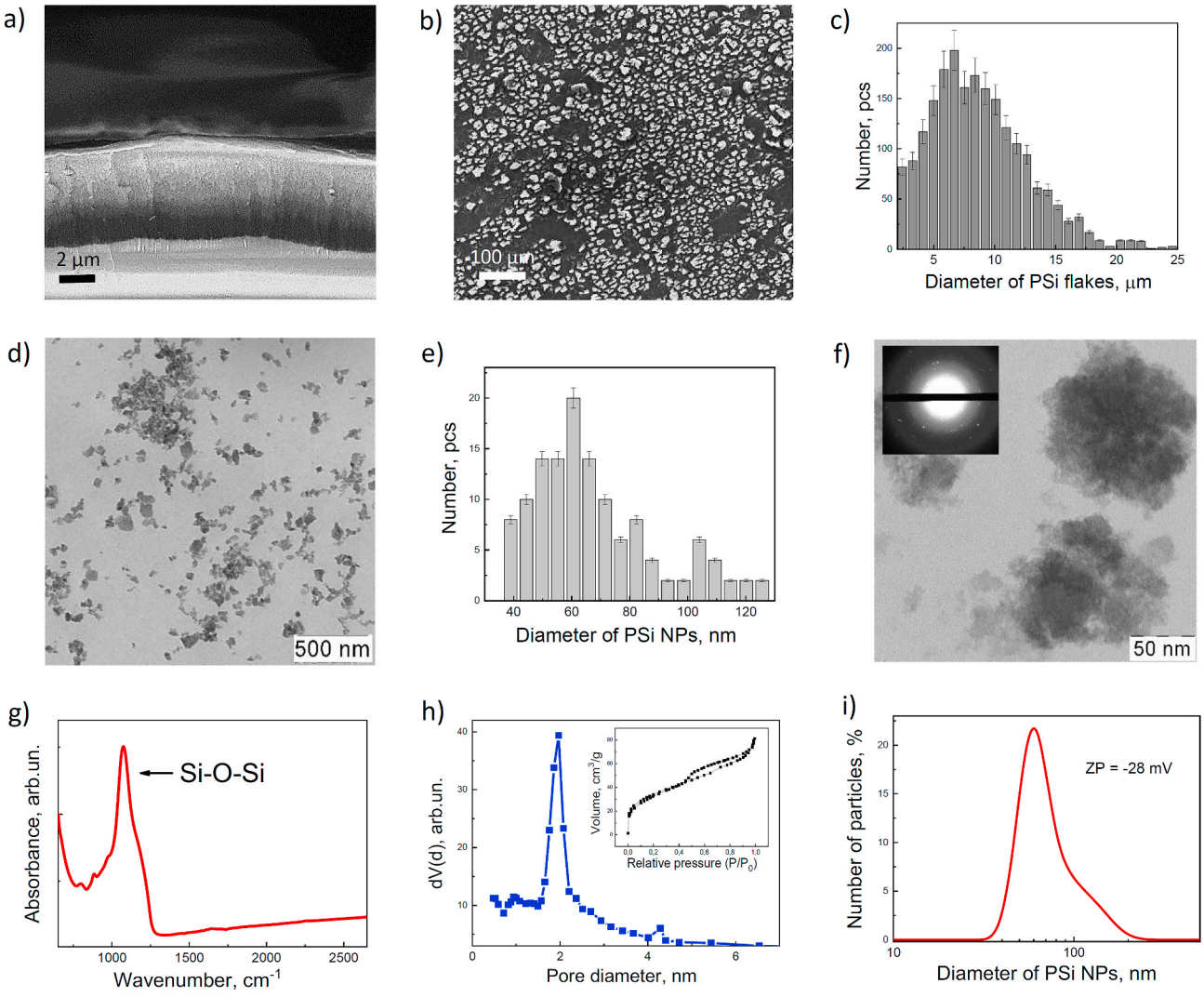

Fig. 2. SEM cross-section microphotograph of PSi film (a); SEM planar microphotograph of PSi flakes (b); PSi flakes size distribution obtained from SEM analysis (c); TEM microphotograph of PSi NPs (d); PSi NPs size distribution obtained from TEM analysis (e); TEM microphotograph of the individual PSi NPs, Inset: pattern of the PSi NPs electron diffraction (f); FTIR absorbance spectra of PSi NPs (g); Pore size distribution in PSi NPs. Inset: nitrogen adsorption/desorption isotherm distribution for PSi NPs (h); size distribution of PSi NPs obtained by DLS (i).

SEM image, was about 6 μm as shown in Fig. 2c.

To obtain stable colloidal solutions of PSi NPs, PSi flakes were ground in water in a ball mill machine and then centrifuged to remove the coarse fraction. Fig. 2d shows TEM microphotograph of the obtained PSi NPs. According to TEM image, the obtained nanoparticles are irregular in shape due to the top-down fabrication process. The mean size of nanoparticles, obtained by the analysis of the TEM image, was 60 nm as presented in Fig. 2e. Fig. 2f shows the resulting PSi NPs with high magnification, at which their microporous structure becomes visible. The presence of diffraction rings in the electron diffraction pattern obtained in the "transmission" geometry for PSi NPs indicates that the nanoparticles consist of a large number of tiny (2–5 nm) silicon nanocrystals [22,50].

FTIR spectra of the dried suspensions of nanoparticles in Fig. 2g demonstrate that the surface of PSi NPs is predominantly covered by oxygen, as evidenced by the absorption peaks of Si–O–Si vibrations at 1070 cm^{-1}. The oxygen coverage of the surface of PSi NPs ensures their hydrophilic properties and determines the possibility to form the stable aqueous suspensions [22]. According to the BET and BJH data (Fig. 2h), PSi NPs have an average pore diameter of 2 nm and a specific surface area of 200 m^2/g. The average hydrodynamic size of PSi nanoparticles shown in Fig. 2i, measured by dynamic light scattering (DLS), demonstrates the size (diameter) distribution of PSi nanoparticles in suspension and is characterized by a maximum of about 60 nm, which is in good agreement with the TEM measurements. The zeta potential (ZP) of PSi NPs is negative and amounts to -28 ± 2 mV.

3.2. ELISA analysis of PSi flakes and PSi NPs H1N1 adsorption activity

The antiviral adsorption activity of PSi flakes with a size of 6 μm and PSi NPs with a size of 60 nm was compared by *ELISA* using the example of H1N1 Influenza A virus (Fig. 3). The concentration of porous particles was 1 mg/ml, the concentration of the virus was varied and amounted to 0.5, 1, 2.5 and 5 μg/ml. Note that a 1 mg/ml viral suspension concentration corresponds to more than 10^9 viral particles per ml (215 hemagglutination units per ml (see SD for details) [51].

According to the results presented, tiny nanoparticles exhibited greater adsorption activity than micrometer flakes for all viral concentrations used. This, apparently, indicates the presence of multiple

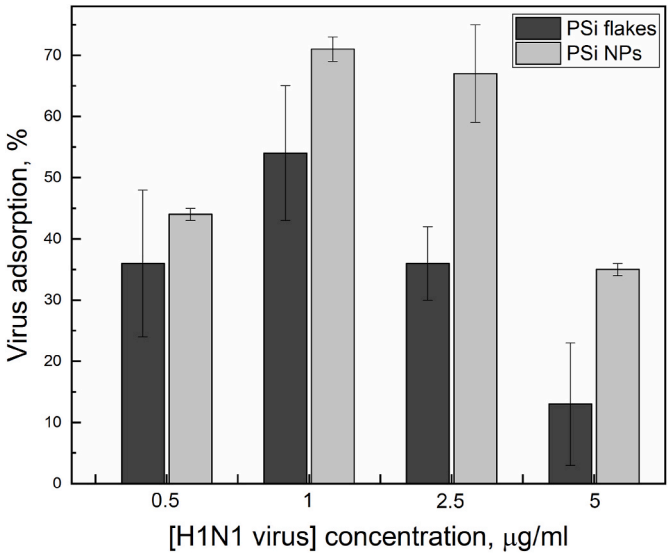

Fig. 3. *ELISA* analysis of antiviral adsorption activity of PSi flakes with a size of 6 μm and PSi NPs with a size of 60 nm to the H1N1 influenza virus. The final concentration of porous particles was 1 mg/ml, incubation time – 20 min, the final concentration of the virus was varied and amounted to 0.5, 1, 2.5 and 5 μg/ml.

interactions with viruses with a decrease in the particle size of microporous silicon. The size of influenza virions is about 100 nm [52], which is commensurate with the size of PSi NPs used in the experiment (60 nm). Apparently, in this case, the formation of agglomerates with virions occurs, and for PSi flakes about 6 μm in size, the surface interaction of viruses with the microporous surface of individual flakes rather occurs.

The maximum adsorption activity for both types of samples was observed when the concentrations of the viruses was 1 μg/ml. Smaller values at higher and lower concentrations indicate the presence of unbound virions. This may be due to the formation of PSi flakes (NPs)- PSi flakes (NPs) agglomerates at low concentrations, and an insufficient number of PSi flakes (NPs) at high concentrations.

The dependence of the antiviral adsorption activity of PSi NPs against the H1N1 influenza virus at different incubation times: 5, 15, 30, and 60 min is shown in SD Fig. S3. The final concentration of nanoparticles was 0.5 mg/ml, the concentration of the virus was 1 or 2.5 μg/ml. According to the results obtained, about 45% of viruses are adsorbed in the first 20–30 min, and during an additional 30 min of incubation (60 min in total), another 15% of virions (about 70% in total) are adsorbed for both concentrations of the virus used. Thus, within 20–30 min, PSi NPs adsorb most of the virions from the contaminated solution. The antiviral adsorption activity of PSi NPs taken at concentrations of 0.05, 0.25, 0.5, 1 and 2.5 mg/ml against the H1N1 influenza virus was also studied (SD Fig. S4). The concentration of the virus in the experiment was 1 or 2.5 μg/ml, the incubation time was 20 min. It is shown that the sorption activity of nanoparticles increases with an increase in their concentration. According to the data presented in Fig. S4, the 50% effective dose (ED_{50}) of PSi NPs, which provides to the binding of 50% of viruses, was about 0.7 mg/ml.

3.3. Registration of virus sizes and virus adsorption by PSi NPs using DLS

DLS spectra of suspensions of various viruses are shown in Fig. 4a. The peaks in the size distribution of virions turned out to be 105 nm for Influenza A virus, 37 nm for Poliovirus, 30 nm for Hepatitis A virus, 50 nm for West Nile virus and 105 nm for Human immunodeficiency virus. Note that the results obtained are in correlation with the encyclopedic data presented in Mahy and Regenmortel 2008 [52].

The study of the interaction of viruses and PSi NPs using DLS is presented in Fig. 4b. According to the presented data, after mixing suspensions of 60 nm nanoparticles and 105 nm of Influenza A virus particles, the maximum size distribution of the mixture shifted to 360 nm (dark blue line in Fig. 4b). The obtained data demonstrate the formation of agglomerates of NPs and virions after their interaction, since the total size of the agglomerates in DLS is larger than the sum of the sizes of NPs and virions obtained separately. The same results were earlier obtained for HIV [28]. Unfortunately, the DLS spectra of PSi NPs mixtures with Poliovirus, Hepatitis A virus, West Nile virus could not be measured due to fast process of their mixture components binding and precipitation.

3.4. Virucidal activity of PSi NPs against different type of pathogenic human virus in-vitro

Antiviral adsorption (virucidal) activity of PSi NPs against to Poliovirus, Hepatitis A virus, West Nile virus, Influenza A virus and Human immunodeficiency virus was studied *in vitro*. For this, the cells were infected with a virus suspension, which was pretreated with PSi NPs: stirring for 20 min and gentle centrifugation for 5 min 2000 rpm. The suspension without NPs treatment was used as a control. Fig. 5 shows the values of the virus titer (log_{10} $TCID_{50}$/ml) of the five studied pathogenic viruses, before and after treatment of virus-contaminated suspensions with PSi NPs.

The virucidal activity of PSi NPs was determined by reducing of the virus titer in viral suspensions after treatment with nanoparticles. Note, that for HIV, after interaction with nanoparticles, the presence of the

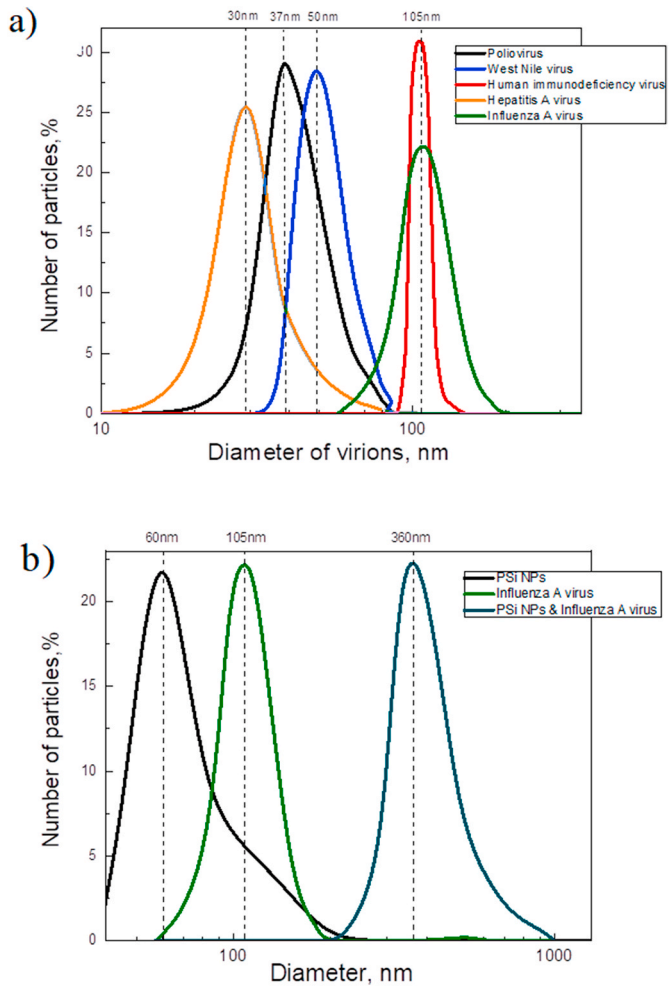

Fig. 4. DLS spectra of Poliovirus, Hepatitis A virus, West Nile virus, Influenza A virus and Human immunodeficiency virus (a); DLS spectra of PSi NPs, Influenza A virus, and the mixture of PSi NPs and Influenza A virus (b).

virus in the experimental group of cells was not detected. Reduction factor (RF) was calculated as the logarithmic titer in the virus control minus the logarithmic titer of the test virus (RF = Δ $\log_{10}$ $TCID_{50}$/ml). According to the data obtained, the infectious titer decreased by approximately 10^4 times (RF ≅ 4 $\log_{10}$ $TCID_{50}$/ml). These values corresponded to an inactivation of 99.99% [53] for all studied viruses and regarding as evidence of universal virucidal activity of PSi NPs.

3.5. Viruses and PSi NPs binding detection using TEM

TEM micrographs were taken to visualize the binding of viruses and PSi NPs. Fig. 6a shows TEM image of negatively stained Influenza A H1N1 viral particles. According to the resulting image, this is an enveloped virus, which looks like spheroidal nanoparticles with sizes about 100 nm in diameter. The Inset to Fig. 6a shows a TEM image of the virus surface, on which membrane glycoproteins, hemagglutinin and neuraminidase [31] are clearly visible. These glycoproteins are key proteins for the reproduction of the Influenza A virus: hemagglutinin is used to enter the cell, and neuraminidase is used to exit it [54].

Fig. 6b shows TEM image of Influenza A virions after interaction with PSi NPs. It can be seen that the interaction of virions with the porous surface of nanoparticles leads to their physical binding and the formation of agglomerates. The presence of characteristic electron diffraction corresponding to silicon nanocrystals taken from Fig. 6b confirms that viruses are indeed surrounded by silicon nanoparticles (Fig. S5).

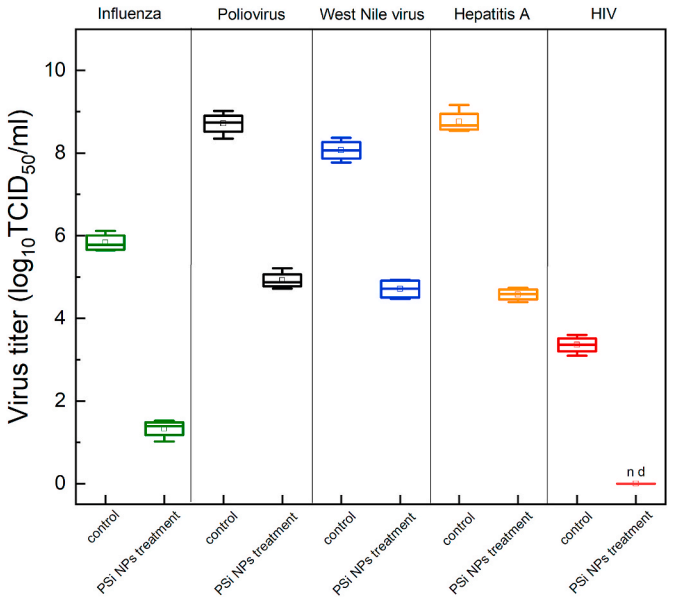

Fig. 5. Virucidal effect of PSi NPs against Influenza A virus, Poliovirus, West Nile virus, Hepatitis A virus, and Human immunodeficiency virus (HIV), which is expressed in a decrease in the titer of the virus after interaction with nanoparticles as compared to the control.

4. Conclusion

In this work, it has been shown that PSi NPs with an average diameter of 60 nm can be easily obtained by grinding of porous silicon films. Nanoparticles are characterized by a microporous structure with an average pore diameter of 2 nm and a specific surface area of 200 m^2/g. *ELISA* tests demonstrated a high antiviral adsorption activity of the obtained nanoparticles: after a short 20 min interaction with 2.5 mg/ml PSi NPs, binding of up to 90% of virions was observed. It has been shown that the dynamic light scattering method can be used to determine the size of various virions. It was also shown by the DLS method that the capture of viruses by PSi NPs is accompanied by the formation of their large agglomerates. The average size of the obtained agglomerates is significantly larger than the size of nanoparticles and viruses separately. We assume that the huge specific surface area of the PSi NPs ensures effective binding of virions. The virucidal activity of PSi NPs was determined by reducing of the virus titer in viral suspensions (Influenza A H1N1 virus, Poliovirus, Human immunodeficiency virus, West Nile virus and Hepatitis virus) after treatment with nanoparticles. According to the data obtained, the infectious titer decreased by approximately 10^4 times, that corresponding to an inactivation of 99.99% for all studied viruses and regarding as evidence of universal virucidal activity of PSi NPs. TEM image reveals that the interaction of virions with the porous surface of nanoparticles leads to their physical binding and the formation of agglomerates. Thus, the virucidal activity of PSi NPs, aimed directly at the virus, is very attractive, since the site of action of the inhibitor is extracellular and, therefore, relatively accessible. The detected antiviral sorption activity of PSi NPs can directly prevent the contact of the virus with host cells, since agglomerates formed after contact with viruses are easily removed from solutions before the infection of host cells, and can be used for purification of water, biopharmaceuticals, donor blood, etc. In subsequent works, the destruction of the viruses, captured by PSi NPs, can be achieved by loading the appropriate drug into the pores of the nanoparticles or using such their properties of photo-, sono- or RF-EM [22] sensitization. Moreover, the demonstrated universal antiviral activity of porous silicon nanoparticles against various pathogenic viruses in the future can be used in the development of first aid equipment in the event of unforeseen viral epidemics or pandemics.

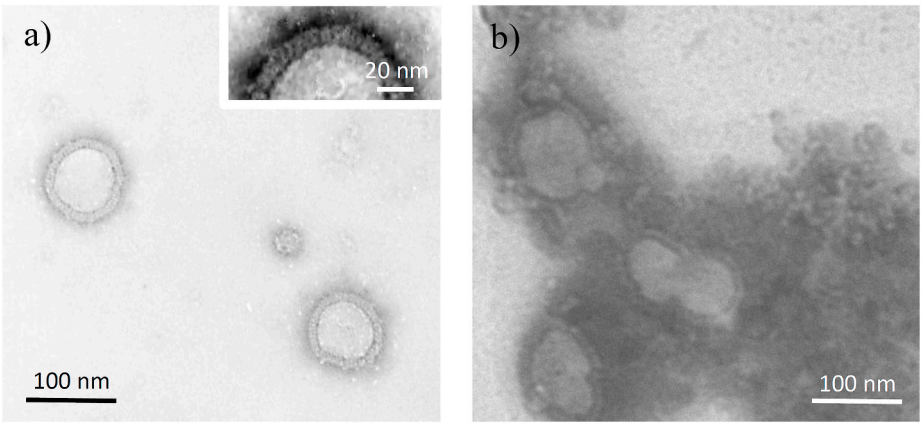

Fig. 6. TEM image of negatively stained Influenza A H1N1 virions; Inset: the closer view of the virion surface (a); TEM image of Influenza virions captured by PSi NPs (b).

Funding

The research was funded by the Russian Science Foundation (Grant number 20-12-00297).

CRediT authorship contribution statement

Liubov A. Osminkina: Conceived the initial ideas, Sample preparation, Conceptualization, Data curation, measurements, Formal analysis, Visualization, Writing – original draft, Writing – review & editing. **Svetlana N. Agafilushkina:** DLS measurements, Formal analysis, Writing – original draft. **Ekaterina A. Kropotkina:** Investigation, in-vitro. **Nikolay Yu Saushkin:** Formal analysis. **Ivan V. Bozhev:** Formal analysis. **Sergei S. Abramchuk:** Formal analysis. **Jeanne V. Samsonova:** Formal analysis. **Alexandra S. Gambaryan:** Investigation, in-vitro.

Declaration of competing interest

The authors declare that they have no known competing financial interests or personal relationships that could have appeared to influence the work reported in this paper.

Acknowledgment

This research was performed according to the Development program of the Interdisciplinary Scientific and Educational School of Lomonosov Moscow State University « Photonic and quantum technologies. Digital medicine». The authors express posthumous gratitude to V. Nikiforov and A. Bychenko for initiating the experiments.

Appendix A. Supplementary data

Supplementary data to this article can be found online at https://doi.org/10.1016/j.bioactmat.2021.06.001.

References

[1] R. Medhi, P. Srinoi, N. Ngo, H.V. Tran, T.R. Lee, Nanoparticle-based strategies to combat COVID-19, ACS Applied Nano Materials 3 (9) (2020) 8557–8580.
[2] J. Gao, H. Gu, B. Xu, Multifunctional magnetic nanoparticles: design, synthesis, and biomedical applications, Accounts Chem. Res. 42 (8) (2009) 1097–1107.
[3] H. Daraee, A. Eatemadi, E. Abbasi, S. Fekri Aval, M. Kouhi, A. Akbarzadeh, Application of gold nanoparticles in biomedical and drug delivery, Artificial cells, nanomedicine, and biotechnology 44 (1) (2016) 410–422.
[4] A.K. Gupta, M. Gupta, Synthesis and surface engineering of iron oxide nanoparticles for biomedical applications, Biomaterials 26 (18) (2005) 3995–4021.
[5] S. Galdiero, A. Falanga, M. Vitiello, M. Cantisani, V. Marra, M. Galdiero, Silver nanoparticles as potential antiviral agents, Molecules 16 (10) (2011) 8894–8918.
[6] V. Cagno, P. Andreozzi, M. D'Alicarnasso, et al., Broad-spectrum non-toxic antiviral nanoparticles with a virucidal inhibition mechanism, Nat. Mater. 17 (2) (2018) 195–203.
[7] D.X. Xiang, Q. Chen, L. Pang, C.L. Zheng, Inhibitory effects of silver nanoparticles on H1N1 influenza A virus in vitro, J. Virol Methods 178 (1–2) (2011) 137–142.
[8] T.Q. Huy, N.T.H. Thanh, N.T. Thuy, P. Van Chung, P.N. Hung, A. T Le, N.T. H. Hanh, Cytotoxicity and antiviral activity of electrochemical–synthesized silver nanoparticles against poliovirus, J. Virol Methods 241 (2017) 52–57.
[9] S. Gaikwad, A. Ingle, A. Gade, M. Rai, A. Falanga, N. Incoronato, L. Russo, S. Galdiero, M. Galdiero, Antiviral activity of mycosynthesized silver nanoparticles against herpes simplex virus and human parainfluenza virus type 3, Int. J. Nanomed. 8 (2013) 4303.
[10] X.X. Yang, C.M. Li, C.Z. Huang, Curcumin modified silver nanoparticles for highly efficient inhibition of respiratory syncytial virus infection, Nanoscale 8 (5) (2016) 3040–3048.
[11] J.C. Trefry, D.P. Wooley, Silver nanoparticles inhibit vaccinia virus infection by preventing viral entry through a macropinocytosis-dependent mechanism, J. Biomed. Nanotechnol. 9 (9) (2013) 1624–1635.
[12] H.A. Jeng, J. Swanson, Toxicity of metal oxide nanoparticles in mammalian cells, J. Environ. Sci. Health Part A 41 (12) (2006) 2699–2711.
[13] O. Bondarenko, K. Juganson, A. Ivask, K. Kasemets, M. Mortimer, A. Kahru, Toxicity of Ag, CuO and ZnO nanoparticles to selected environmentally relevant test organisms and mammalian cells in vitro: a critical review, Arch. Toxicol. 87 (7) (2013) 1181–1200.
[14] Z. Ferdous, A. Nemmar, Health impact of silver nanoparticles: a review of the biodistribution and toxicity following various routes of exposure, Int. J. Mol. Sci. 21 (7) (2020) 2375.
[15] N. Khlebtsov, L. Dykman, Biodistribution and toxicity of engineered gold nanoparticles: a review of in vitro and in vivo studies, Chem. Soc. Rev. 40 (3) (2011) 1647–1671.
[16] J.K. Crane, Metal nanoparticles in infection and immunity, Immunol. Invest. 49 (7) (2020) 794–807.
[17] P. Maximchik, K. Tamarov, E.V. Sheval, E. Tolstik, T. Kirchberger-Tolstik, Z. Yang, V. Sivakov, B. Zhivotovsky, L.A. Osminkina, Biodegradable porous silicon nanocontainers as an effective drug carrier for regulation of the tumor cell death pathways, ACS Biomater. Sci. Eng. 5 (11) (2019) 6063–6071.
[18] F. Peng, Y. Su, X. Wei, Y. Lu, Y. Zhou, Y. Zhong, S.-T. Lee, Y. He, Silicon-nanowire-based nanocarriers with ultrahigh drug-loading capacity for in vitro and in vivo cancer therapy, Angew Chem. Int. Ed. Engl. 52 (5) (2013), 1457–61.
[19] A. Tzur-Balter, G. Shtenberg, E. Segal, Porous silicon for cancer therapy: from fundamental research to the clinic, Rev. Chem. Eng. 31 (3) (2015) 193–207.
[20] S.P. Low, N.H. Voelcker, Biocompatibility of porous silicon, in: Handbook of Porous Silicon, Springer, 2014, pp. 381–393.
[21] E. Tolstik, L. Osminkina, D. Akimov, M. Gongalsky, A. Kudryavtsev, V. Timoshenko, R. Heintzmann, V. Sivakov, J. Popp, Linear and non-linear optical imaging of cancer cells with silicon nanoparticles, Int. J. Mol. Sci. 17 (9) (2016) 1536.
[22] L.A. Osminkina, M.B. Gongalsky, Porous silicon suspensions and colloids, in: L. Canham (Ed.), Handbook of Porous Silicon, Springer, Cham, 2018.
[23] L. Canham, Routes of formation for porous silicon, in: L. Canham (Ed.), Handbook of Porous Silicon, Springer, Cham, 2018.
[24] V. Lehmann, R. Stengl, A. Luigart, On the morphology and the electrochemical formation mechanism of mesoporous silicon, Mater. Sci. Eng., B 69 (2000) 11–22.
[25] S.N. Agafilushkina, O. Žukovskaja, S.A. Dyakov, K. Weber, V. Sivakov, J. Popp, D. Cialla-May, L.A. Osminkina, Raman signal enhancement tunable by gold-covered porous silicon films with different morphology, Sensors 20 (19) (2020) 5634.
[26] J.L. Coffer, L.T. Canham, Nanoporous silicon as a green, high-tech educational tool, Nanomaterials 11 (2021) 553.

[27] J. Rouquerol, D. Avnir, C.W. Fairbridge, D.H. Everett, J.H. Haynes, N. Pernicone, J. D.F. Ramsay, K.S.W. Sing, K.K. Unger, Recommendations for the characterization of porous solids, Pure Appl. Chem. 66 (1994) 1739–1758.
[28] L.A. Osminkina, V.Y. Timoshenko, I.P. Shilovsky, G.V. Kornilaeva, S. N. Shevchenko, M.B. Gongalsky, K.P. Tamarov, S.S. Abramchuk, V.N. Nikiforov, M. R. Khaitov, E.V. Karamov, Porous silicon nanoparticles as scavengers of hazardous viruses, J. Nanoparticle Res. 16 (6) (2014) 1–10.
[29] K.A. Gonchar, S.N. Agafilushkina, D.V. Moiseev, I.V. Bozhev, A.A. Manykin, E. A. Kropotkina, A.S. Gambaryan, L.A. Osminkina, H1N1 influenza virus interaction with a porous layer of silicon nanowires, Mater. Res. Express 7 (3) (2020), 035002.
[30] M.B. Gongalsky, U.A. Tsurikova, J.V. Samsonova, G.Z. Gvindzhiliiia, K.A. Gonchar, N.Y. Saushkin, A.A. Kudryavtsev, E.A. Kropotkina, A.S. Gambaryan, L. A. Osminkina, Double etched porous silicon nanowire arrays for impedance sensing of influenza viruses, Results in Materials 6 (2020), 100084.
[31] D.P. Nayak, R.A. Balogun, H. Yamada, Z.H. Zhou, S. Barman, Influenza virus morphogenesis and budding, Virus Res. 143 (2) (2009) 147–161.
[32] E.C. Hutchinson, Influenza virus, Trends Microbiol. 26 (9) (2018) 809–810.
[33] J.K. Taubenberger, D.M. Morens, The pathology of influenza virus infections, Annu. Rev. Pathol. 3 (2008) 499–522.
[34] C. Butan, D.J. Filman, J.M. Hogle, Cryo-electron microscopy reconstruction shows poliovirus 135S particles poised for membrane interaction and RNA release, J. Virol. 88 (3) (2014) 1758–1770.
[35] World Health Organization, Poliomyelitis, Dec 2019, https://www.who.int/en/news-room/fact-sheets/detail/poliomyelitis.
[36] S.T. Al Awaidy, F. Khamis, Wild Poliovirus Type 1 in Oman: a re-emerging threat that requires urgent, targeted and strategic preparedness, Sultan Qaboos University Medical Journal 20 (1) (2020) e1–e4.
[37] J.A. Briggs, T. Wilk, R. Welker, H.G. Kräusslich, S.D. Fuller, Structural organization of authentic, mature HIV-1 virions and cores, EMBO J. 22 (7) (2003) 1707–1715.
[38] C.B. Wilen, J.C. Tilton, R.W. Doms, HIV: cell binding and entry, Cold Spring Harbor perspectives in medicine 2 (8) (2012) a006866.
[39] World Health Organization, New guidance on ethical HIV prevention trials. https://www.who.int/news/item/27-01-2021-new-guidance-on-ethical-hiv-prevention-trials-. (Accessed January 2021).
[40] S. Mukhopadhyay, B.S. Kim, P.R. Chipman, M.G. Rossmann, R.J. Kuhn, Structure of west nile virus, Science 302 (5643) (2003), 248-248.
[41] R. Kanai, K. Kar, K. Anthony, L.H. Gould, M. Ledizet, E. Fikrig, W.A. Marasco, R. A. Koski, Y. Modis, Crystal structure of West Nile virus envelope glycoprotein reveals viral surface epitopes, J. Virol. 80 (22) (2006) 11000–11008.
[42] T. Bakonyi, J.M. Haussig, West Nile virus keeps on moving up in Europe, Euro Surveill. 25 (46) (2020), 2001938.
[43] E.H. Cook Jr., D.W. Bradley, C.R. Gravelle, J.E. Maynard, Ultrastructural studies of hepatitis A virus by electron microscopy, J. Virol. 20 (3) (1976) 687.
[44] R.S. Koff, Hepatitis a. Lancet 351 (1998), 16439.3.
[45] X. Wang, J. Ren, Q. Gao, Z. Hu, Y. Sun, X. Li, D.J. Rowlands, W. Yin, J. Wang, D. I. Stuart, Z. Rao, E.E. Fry, Hepatitis A virus and the origins of picornaviruses, Nature 517 (7532) (2015) 85–88.
[46] F. Deinhardt, Prevention of viral hepatitis A: past, present and future, Vaccine 10 (1992) S10–S14.
[47] M.G. Hofmeister, J. Xing, M.A. Foster, R.J. Augustine, C. Burkholder, J. Collins, S. McBee, E.D. Thomasson, D. Thoroughman, M.K. Weng, P.R. Spradling, Hepatitis A person-to-person outbreaks: epidemiology, morbidity burden, and factors associated with hospitalization—multiple states, 2016–2019, J. Infect. Dis. 223 (3) (2021) 426–434.
[48] G. Sofer, Virus inactivation in the 1990s—and into the 21st century, Biopharm Int. 16 (2003) 50–57.
[49] R. Walter, W. Macht, J. Dürkop, R. Hecht, U. Hornig, P. Schulze, Virus levels in river waters, Water Res. 23 (2) (1989) 133–138.
[50] G. Ledoux, O. Guillois, D. Porterat, C. Reynaud, F. Huisken, B. Kohn, V. Paillard, Photoluminescence properties of silicon nanocrystals as a function of their size, Phys. Rev. B 62 (23) (2000) 15942.
[51] P. Kramberger, M. Ciringer, A. Štrancar, M. Peterka, Evaluation of nanoparticle tracking analysis for total virus particle determination, Virol. J. 9 (1) (2012) 1–10.
[52] B.W. Mahy, M.H. Van Regenmortel, Encyclopedia of Virology, Academic Press, 2008.
[53] M. Eggers, M. Eickmann, J. Zorn, Rapid and effective virucidal activity of povidone-iodine products against Middle East respiratory syndrome coronavirus (MERS-CoV) and modified vaccinia virus Ankara (MVA), Infectious diseases and therapy 4 (4) (2015) 491–501.
[54] S.J. Gamblin, J.J. Skehel, Influenza hemagglutinin and neuraminidase membrane glycoproteins, J. Biol. Chem. 285 (37) (2010) 28403–28409.